Photo-induced lattice distortion in 2H-$MoTe_2$ probed by time-resolved core level photoemission

R. Costantini, [a] F. Cilento, [b] F. Salvador,[a] A. Morgante, [ac] G. Giorgi, [de] M. Palummo [f] and M. Dell'Angela *[a]

Received 29th November 2021, Accepted 2nd March 2022

The technological interest in $MoTe_2$ as a phase engineered material is related to the possibility of triggering the 2H–1T′ phase transition by optical excitation, potentially allowing for an accurate patterning of metallic areas into a semiconducting canvas *via* laser irradiation. In this paper, we investigate the photo-induced modifications of a bulk 2H-$MoTe_2$ crystal by means of time-resolved X-ray photoemission spectroscopy. We observe that in the microsecond timescale, the core levels shift to higher kinetic energies due to surface photovoltage fields, while in the sub-nanosecond range, the photoemission peaks shift in the opposite direction. With the support of DFT calculations, we ascribe the latter effect to the deformation of the lattice in the out-of-plane direction, which is along the pathway for the 2H–1T′ phase transition. Our data indicate an intermediate lattice excitation state with a measured lifetime in the order of 600 ps, in which the displacement of Mo and Te atoms causes the Te 4d electrons to shift towards higher binding energies.

Introduction

Transition metal dichalcogenides (TMDs) have been widely explored for the development of innovative nanoscale devices. TMDs are compounds with layered structures, with each layer consisting of a three atom unit (MX_2) with a transition metal atom (M) sandwiched between two chalcogen layers (X = S, Se, Te). The multiple combinations of transition metal and chalcogen atoms in TMDs result in a large range of electronic properties, which also depend on the crystal phase

[a]*CNR-IOM Laboratorio TASC, SS 14 Km 163.5, I-34149 Trieste, Italy. E-mail: dellangela@iom.cnr.it*
[b]*Elettra Sincrotrone Trieste S.C.p.A., Strada Statale 14 Km 163.5, I-34149 Trieste, Italy*
[c]*Department of Physics, University of Trieste, Via A. Valerio 2, I-34127 Trieste, Italy*
[d]*Department of Civil and Environmental Engineering (DICA), University of Perugia, Via G. Duranti 93, I-06125 Perugia, Italy*
[e]*CNR-SCITEC, I-06123 Perugia, Italy*
[f]*Dipartimento di Fisica, INFN, Università di Roma "Tor Vergata", Via della Ricerca Scientifica 1, 00133 Roma, Italy*

and on the sample thickness.[1] The indirect gap of bulk TMDs becomes direct when thinned down to monolayers, and the material character can change from semiconducting to (semi-)metallic if the trigonal prismatic (1H/2H) phase is distorted into an octahedral (1T/1T′) structure.

Molybdenum ditelluride ($MoTe_2$) is a prototypical TMD. It presents two crystal structures at room temperature: the semiconducting hexagonal phase (2H or α-phase) and the semimetallic monoclinic phase (1T′ or β-phase). In its 2H phase, $MoTe_2$ has attracted significant interest from a technological point of view due to its bandgap in the near infrared region (0.9 eV in the bulk and 1.1 eV in the monolayer), which makes it a potential alternative to silicon for optoelectronic applications. Very recently, carrier multiplication has been demonstrated in 2H-$MoTe_2$, making it a promising material for the development of light harvesting devices.[2] The 1T′ phase of $MoTe_2$ is metastable, since a barrier of around 0.7 eV (ref. 3 and 4) impedes the reconversion of the system to the 2H phase, making this material a promising template for relevant phase engineering applications.[5,6] Laser induced phase patterning has in fact been successfully applied to $MoTe_2$ to fabricate an ohmic heterophase homojunction.[7] The use of optical excitations allows for a precise transformation of the structural properties of the substrate with high area and phase selectivity, which is not achievable with traditional thermal and strain treatments.

The microscopic nature of the 2H–1T′ photo-induced phase transition in $MoTe_2$ is still debated. Several studies have recently tackled the photoexcited carrier dynamics in 2H-$MoTe_2$ by means of optical, terahertz, electron and X-ray spectroscopies.[8–11] It has been shown that photoexcitation is followed by thermalization of the lattice within 2 ps and the subsequent cooling process of the phonons occurs in the 100 ps timescale.[10] MeV ultrafast electron diffraction experiments have shown that by tuning the excitation wavelength, it is possible to control the evolution of the phonon populations by coupling to zone-center or zone-edge vibrational modes and, therefore, to control the structural dynamics.[12] More recently, a theoretical work has demonstrated that the photo-induced transition from 2H to 1T′ in $MoTe_2$ monolayers is purely triggered by electronic excitation, which causes the softening of the A''_2 phononic mode, provided that the pump energy is above 1.96 eV.[13]

In this work, we study the structural dynamics of an optically excited 2H-$MoTe_2$ single crystal by means of time-resolved X-ray photoemission spectroscopy (tr-XPS). We use laser pulses with a photon energy of 2.4 eV as a pump and synchrotron X-ray pulses as a probe. We show that the optical excitation results in the accumulation of electrons in the top layer, generating a long-lived surface photovoltage (SPV), which causes the shift of the photoelectron spectra to lower binding energies, as compared to those of the unpumped system. Conversely, on the sub-nanosecond timescale, we observe a transient shift of the Te 4d core level to positive binding energies, which cannot be ascribed to the SPV. We used DFT calculations to simulate the deformation of the lattice along the A''_2 mode of the monolayer, corresponding to an out-of-plane displacement of Mo and Te atoms moving in opposite directions. The theoretical model shows that an atomic displacement of the order of 0.01 Å suffices to cause a ∼10 meV positive binding energy shift, in agreement with the experimental data. The fingerprints of this transient distortion are spectroscopically inequivalent to those of the irreversible 2H-to-1T′ transition. We therefore suggest that this core level shift is due to

a different and reversible structural distortion of the irradiated sample, which recovers in the 600 ps timescale.

Experimental details

Materials and methods

The 2H-$MoTe_2$ crystal (>99.995% purity) was purchased from HQ Graphene (Groningen, the Netherlands) and cleaved in an ultra-high vacuum (base pressure in the experimental chamber $<3 \times 10^{-10}$ mbar). All measurements were carried out at the ANCHOR-SUNDYN endstation of the ALOISA beamline at the Elettra synchrotron in Trieste, Italy.[14] 2.4 eV (515 nm) pulses from an Yb-doped yttrium aluminum garnet (Yb:YAG) fiber laser (Tangerine HP, Amplitude Systèmes, Pessac, France) were used as a pump to excite the samples. The laser was operated at 385.67 kHz and was used to pump one out of every three hybrid X-ray pulses of the storage ring (1.157 MHz), as detailed in ref. 15. The X-ray and optical beams were impinging on the sample in a quasi-collinear geometry, and the spatial overlap was preliminarily determined on a YAG crystal mounted on the sample holder. XPS spectra in the pump on/pump off series were acquired with a photon energy of 400 eV and a pass energy of 20 eV. As such scans were acquired using the multibunch radiation of Elettra, the pump-induced effects were averaged on a 2.6 μs delay range, *i.e.*, the separation between consecutive laser pulses. By acquiring the scans in pump off/pump on sequences, we ensured the reversibility of the effect and excluded radiation damage. Time-resolved spectra were acquired with the pump laser synchronized to 150 eV synchrotron probe pulses. The temporal coincidence of the pump and probe pulses was calibrated by measuring the surface photovoltage shift on a silicon crystal. Considering the significant difference in pulse duration for the pump (∼300 fs) and the probe (∼100 ps) pulses, the latter dominates the cross-correlation, and therefore the temporal resolution in time-resolved XPS measurements.

Theoretical methodology

Geometric structures were optimized and single-point calculations of the $MoTe_2$ monolayers (see Fig. 1) were performed by means of density functional theory (DFT), as implemented in the VASP code,[16–19] within the generalized gradient approximation (GGA) of Perdew–Burke–Ernzerhof (PBE).[20] The ion–electron interactions were described by the projector augmented wave (PAW) method.[21] A plane-wave basis set energy cutoff of 600 eV was employed. Also, the zero damping DFT-D3 (Becke–Johnson) method of Grimme was employed to include the long-range interactions.[22] As an initial model, we employed the three-atom unit cell (1 Mo, 2 Te) of the ML, whose Brillouin zone (BZ) was sampled with a Γ-centered k-point mesh of $24 \times 24 \times 1$. A sufficient amount of vacuum was added along the non-periodic direction to avoid any possible spurious interaction among replicas. Any possible residual dipole along the same non-periodic direction was properly corrected. Optimizations were carried out until residual forces were below 0.005 eV $Å^{-1}$. The optimized lattice parameters and angles of the ML are $a = b =$ 3.4996 Å and $\alpha = \beta = 90^\circ$ and $\gamma = 120^\circ$.

We then calculated the changes in the core level energies according to the final state effect scheme, which consisted of isolating one atom and creating a core

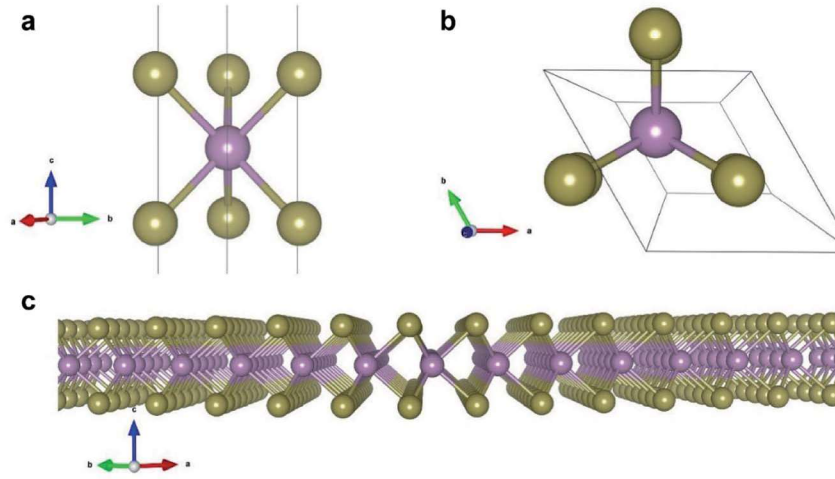

Fig. 1 Lateral (a) and top (b) view of the optimized structure of the ML of $MoTe_2$. (c) Lateral view of the supercell of the same ML of $MoTe_2$. Purple: Mo; gold: Te.

hole and injecting the electron back into the empty states;[23] in our calculations, we focused on Te 4d electrons. Convergence of the calculations was checked up to 8×8 supercells (128 Te & 64 Mo atoms).

Results and discussion

We measured the effects of the optical excitation on the 2H-$MoTe_2$ crystal core levels, from the sub-nanosecond to the microsecond timescale. We first acquired photoemission spectra in the Mo 3d and Te 4d ranges by optically exciting the sample with 2.4 eV photons and detecting the photoelectrons generated by the whole multibunch radiation of the Elettra synchrotron. The pump-induced effects in this case are averaged over the time between consecutive laser pulses, as described in the Methods section. If compared to the actual time-resolved XPS scans, which are presented later in the text, this acquisition method ensures a higher count rate and can be used to quickly assess the presence of long-lived effects and the entity of the possible radiation damage caused by the laser (not detected in this experiment). Fig. 2 shows the Mo 3d and Te 4d core levels as a function of the applied laser fluence. The spectra were acquired by alternating pump-off and pump-on scans while increasing the laser power to examine whether any irreversible changes had been introduced. Below 0.4 mJ cm^{-2} all pump-induced effects are completely reversible and consist of: (i) a rigid shift of the Mo 3d and Te 4d lines to lower (higher) binding (kinetic) energies, (ii) the appearance of a weak component ~0.6 eV below the Mo $3d_{5/2}$ peak, as indicated by the black arrow and (iii) the reduction of the Te 4d peak intensity. By switching the laser off, the spectrum returns to its original shape, thus, we only show the first of the unpumped spectra for clarity. Above 0.4 mJ cm^{-2}, the appearance of the novel component (ii) becomes persistent even after switching off the optical excitation. The energy position of (ii) is compatible with Mo $3d_{5/2}$ photoelectrons from Mo atoms in the 1T′ phase.[7,24] Concurrently, we would expect its Mo $3d_{3/2}$

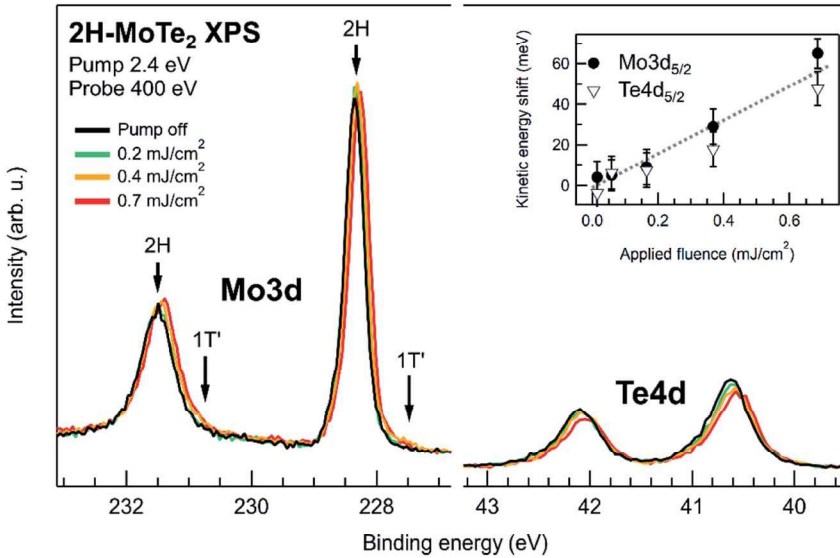

Fig. 2 Mo 3d and Te 4d photoemission lines as a function of the applied laser fluence. The pump photon energy is 2.4 eV and the probe photon energy is 400 eV. The spectra shift consistently to lower binding energies with increasing fluence due to the surface photovoltage caused by the long-lived charge carriers. The components of the Mo 3d core level assigned to the 2H and 1T′ phases are also labelled. The inset shows the energy shift of Mo $3d_{5/2}$ and Te $4d_{5/2}$ as a function of the applied fluence with respect to the laser off spectra.

counterpart and a Te 4d doublet with a ~0.6 eV lower binding energy with respect to the original Te 4d lines; due to the larger intrinsic width of the Mo $3d_{3/2}$ and Te 4d peaks and the weak intensity of the 1T′ component (~2.5% with respect to the pristine 2H-$MoTe_2$, as derived from the fits), such contributions do not emerge as clearly as for Mo $3d_{5/2}$ in the current dataset. The slight broadening of the Te 4d lines, however, is consistent with the appearance of a chemically inequivalent component near the 2H related peak. Moreover, the decreasing intensity of Te 4d (iii) as a function of the increasing pump fluence is a further proof of a partial 2H-to-1T′ transition, since the 1T′ phase is also characterized by Te vacancies.[7,24] Indeed, the diffusion and ordering of Te vacancies is one of the proposed mechanisms for the 2H-to-1T′ phase transition.[11,25]

The last optically induced effect to be discussed is the spectral shift to higher kinetic energies (i). Due to the semiconducting properties of 2H-$MoTe_2$, we ascribe this shift to the surface photovoltage arising after the separation of the photogenerated excitons. The direction of the shift indicates that the material is a p-type semiconductor; even though the material is intrinsically n-type, it has been shown that exposure to air and the presence of adsorbates converts $MoTe_2$ into a p-type semiconductor,[26] in agreement with our observations. It was also shown that in order to restore the original n-type conductance of the material, an annealing of the crystal at 350 K in a vacuum is necessary.[26] This fact led us to conclude that the pump fluences used in our experiments, which were all conducted at room temperature, did not cause a significant temperature increase in the sample.

The shift amplitude as a function of the applied fluence is shown in the inset of Fig. 2. The trend appears to be linear, despite the expected dependency of SPV induced shifts on the laser power being logarithmic.[27] To evaluate the excited carrier density in $MoTe_2$, we should consider the saturable absorption correction, which reduces the absorption coefficient according to:

$$\alpha = \frac{\alpha_0}{1 + \frac{I}{I_S}}$$

where α and α_0 are the absorption coefficients with and without saturable absorption effects, respectively, I is the incident peak intensity and I_S is the saturation peak intensity. The latter quantity has been reported for 2H-$MoTe_2$ and a 300 fs pulse at 515 nm,[28] and amounts to ~60 GW cm^{-2}. In our experiments, the peak power at 0.7 mJ cm^{-2} fluence is ~2 GW cm^{-2}, which gives the lowest α/α_0 ratio of 0.97; we can therefore neglect saturable absorption effects in the evaluation of the excited carrier density. From the optical properties of $MoTe_2$ (ref. 29), we find a reflectivity $R = 0.44$ at normal incidence and a penetration depth of ~2 × 10^{-4} cm, which gives an upper limit for the excited carrier density of ~5 × 10^{18} cm^{-3} with an applied fluence of 0.7 mJ cm^{-2}, assuming one excited electron per absorbed photon. For photon energies larger than twice the band gap (~1 eV for bulk $MoTe_2$ (ref. 30)) quantum yields of 1.5–2 have been observed,[31] raising the upper limit of the excited carrier density to ~1 × 10^{19} cm^{-3} in our measurements. Considering that 2H-$MoTe_2$ has 18 valence electrons per unit cell (*i.e.*, in a volume of ~1.7 × 10^{22} cm^3), we get a maximum excitation density[32] of 0.01%. Moreover, if we assume a uniform absorption in the interaction volume and a monolayer thickness of 0.7 nm, we obtain an average of ~7 × 10^{11} cm^{-2} carriers per layer, which is lower than the Mott threshold of ~1 × 10^{13} cm^{-2} reported for other TMDs.[33,34] On one hand, these low numbers are in agreement with the observed SPV linear trend; on the other hand, this estimate disagrees with the requirement of a threshold concentration of carriers for the 2H-to-1T′ transition to occur,[13] since the fingerprints of both the Te vacancies and the 1T′ component in the Mo 3d region become noticeable at 0.4 mJ cm^{-2}. A plausible explanation for this unexpected behaviour is that higher concentrations of carriers are accumulated at the surface of the material after the separation of the excitons that are generated in the interaction volume, therefore locally triggering the phase transition. This mechanism has been recently observed in 2H-MoS_2, in which the transition to the 1T metallic phase is reversible.[35]

The measurements presented in Fig. 2 characterize the photoexcited system in the microsecond range, therefore they define the SPV corrected position of the core levels acquired in the sub-nanosecond XPS measurement. The concept is summarized in Fig. 3. The static XPS spectrum acquired without optical excitation (a) serves as a reference for the absolute binding energy positions of the core levels. The measurement has then been repeated while illuminating the sample with increasing optical fluence, but without synchronizing the pump and probe sources (b). In these measurements, the pump-induced effects are averaged over 2.6 μs, which is the time separation between two consecutive laser pulses; as we have shown in Fig. 2, the dominant effect is the SPV shift to lower binding energies. Finally, we performed the time-resolved scans by synchronizing the laser to the hybrid pulses of the Elettra storage ring[14] and progressively varying the delay between the two (c). We observed

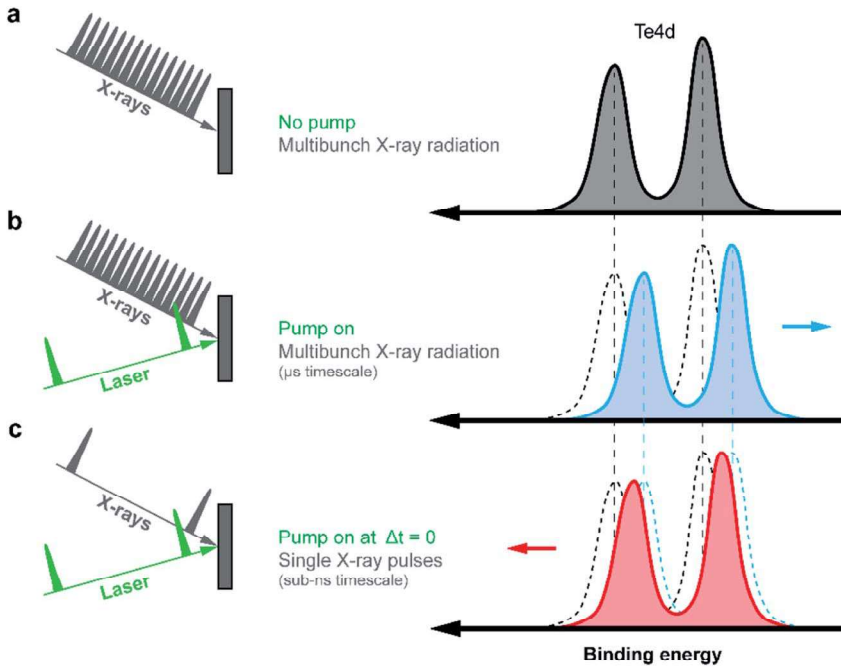

Fig. 3 Scheme of the acquisition modes. (a) The reference spectrum of the Te 4d multiplet is acquired without optical excitation (black) to define the reference binding energy of the peaks. (b) A series of spectra as a function of the applied laser fluence (blue) is acquired using the multibunch radiation as a probe, in order to detect the average optically induced modification in the system in the microsecond range. The peaks shift to lower binding energies due to the surface photovoltage, as indicated by the blue arrow. (c) The time-resolved XPS experiment is performed using the single X-ray pulses as a probe, unveiling the photo-induced dynamics in the sub-nanosecond range (red). The red arrow indicates that the spectral shift in this case is towards positive binding energies, suggesting that the origin of the effect is different from the photovoltage effect that is present at longer delay times.

that when the pump and probe pulses are temporally overlapped, the core levels shift to higher binding energies which, interestingly, is the opposite direction of the SPV effect occurring at longer delay times.

These results are shown in Fig. 4 for the Te $4d_{5/2}$ core level. In particular, the system is excited with 2.4 eV laser pulses at a 0.7 mJ cm^{-2} fluence and probed with 150 eV synchrotron pulses; the laser repetition rate being 1/3 of the synchrotron revolution frequency allows for the parallel acquisition of the photoelectron signal generated by the pumped synchrotron pulse, and a reference signal generated by the subsequent X-ray pulse, *i.e.*, ~0.9 μs after the optical pump, which is used for normalization (when the timescales of the observed effect are short enough). In Fig. 4a, we refer to the former as the "pumped" signal (red trace) and to the latter as the "unpumped" signal (blue trace). In this case, the unpumped trace is equivalent to a "laser on" spectrum at the same pump fluence, therefore it shifted to lower binding energies according to the SPV effect, while the pumped trace displays the dynamics occurring on top of the SPV on shorter timescales. In the bottom panel of Fig. 4a, we also present the false color map of

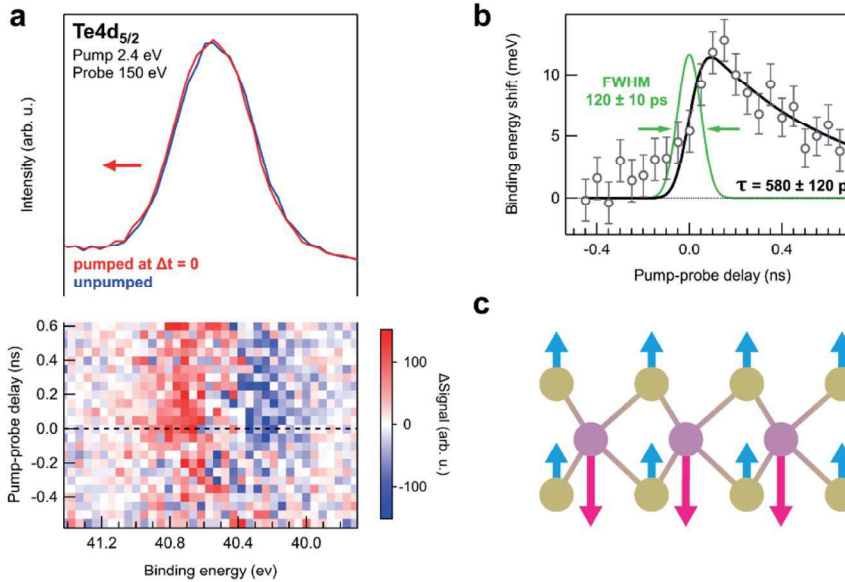

Fig. 4 Time-resolved XPS measurements on the Te $4d_{5/2}$ core level. (a) The unpumped (blue trace) and pumped (red trace) spectra are shown, revealing a rigid shift of the photoemission peak to higher binding energies. A false color map of the difference between the pumped and unpumped signal as a function of the pump–probe delay is also shown, evidencing the shift of the center of mass of the peak after the photoexcitation. (b) Te 4d binding energy shift (circles) obtained by fitting the experimental data for each delay point. The data is fitted by the convolution of a Gaussian peak and an exponential decay (black trace). The Gaussian (green trace) FWHM is held to 120 ps to account for the cross correlation between the pump and probe pulses. The exponential decay yields a time constant of 580 $\pm$ 120 ps. (c) Sketch of the A''_2-like displacements applied in the $MoTe_2$ layer to simulate the chemical shift observed experimentally. Note that the Mo displacement is twice that of Te. Purple: Mo; gold: Te.

the difference between the pumped and unpumped scans for each delay point, from which the shift of the center of mass of the Te $4d_{5/2}$ peak to higher binding energies clearly emerges. In Fig. 4b we show the binding energy shift (circles) as a function of the pump–probe delay that has been obtained by fitting the Te 4d multiplet with a Doniach–Sunjic pair. In particular, the magnitude of the shift is the difference between the binding energies of the pumped and unpumped data at each delay point, meaning that the shift is corrected for any eventual photon energy drift of the synchrotron beam that may occur over the scan acquisition time. The same procedure has been used to derive the broadening and the intensity change of the Te $4d_{5/2}$ peak, revealing no significant variations; the photo-induced effects in the sub-nanosecond range therefore consist of a rigid shift of the core levels to higher binding energies. To derive the lifetime of this effect, we fitted the data points of Fig. 4b using the convolution of and exponential decay with a Gaussian function, to account for the instrumental response function. In particular, the Gaussian FWHM of the fit is held to 120 ps since this value should correspond to the cross-correlation between the pump and probe pulses, which has been independently determined by measuring the SPV dynamics on

a Si crystal under identical experimental conditions. The recovery dynamics of the binding energy shift derived from the fits are therefore well described by a single exponential decay with $\tau = 580 \pm 120$ ps.

As already mentioned, the most interesting aspect of this sub-nanosecond effect is the direction of the shift, which is opposite to the one of the SPV induced shift. In fact, if we suppose that the sub-nanosecond shift is also due to the SPV, we would expect it to be in the same direction of the shift measured in the microsecond range. Even assuming a SPV that has not completely relaxed in the time elapsed between consecutive pump pulses, we should measure a positive (in the case of a p-doped semiconductor) binding energy shift also around time zero.[36–38] We also exclude vacuum space-charge effects[39,40] because the number of secondary electrons photoemitted by the pump pulse is negligible, and because the typical fingerprint of such an effect is a positive kinetic energy shift. The nature of the shift observed in Fig. 4 must therefore be different. Considering the timescales of hundreds of picoseconds, a plausible hypothesis is that lattice related effects are involved. Ultrafast electron diffraction measurements have recently revealed how hot carriers can couple to high-energy phonons, leading to lattice displacements;[12] long-lived lattice heat effects have also been detected in transient X-ray absorption measurements,[8,9] and lattice cooling time constants in the order of 200 ps have been measured by transient optical absorption.[10]

We performed DFT calculations to examine the possibility that the sub-nanosecond shift in our measurement is indeed due to the modification of the chemical environment of the Te 4d electrons that occurs as a consequence of lattice distortion. As an example, the thermally induced lattice expansion in a Ta(100) crystal was experimentally observed to cause a ~30 meV increase in the Ta 4f binding energy.[41] In our case, we model the lattice distortion along the A''_2 phononic mode of the monolayer, displacing Mo and Te atoms in opposite directions along the *c* axis (see Fig. 4c). This is the mode dominating the distortion for photoexcitation with pump photon energies near 2.4 eV,[13] although we acknowledge that in the real system, other phononic modes may also contribute to the lattice distortion. We also underline that in our study, the DFT calculations have been performed on monolayer 2H-$MoTe_2$ and not on a bulk sample, as in the experiment. Despite the different electronic and vibrational properties of monolayer and bulk $MoTe_2$, both undergo the same 2H–1T′ structural transition and we assume that the direction of the core level binding energy shifts of the distorted structure is maintained. The results of our simulations are reported in Table 1. In detail, we observe that the calculated binding energy difference (ΔBE) of the Te 4d

Table 1 Mo and Te displacements along the *c* axis and relative binding energy variations (ΔBE) compared to the unperturbed initially optimized case

Displacement along the *c* axis (Å)		
Mo	Te	ΔBE (eV)
−0.025	+0.0125	0.03
−0.05	+0.025	0.06
−0.10	+0.05	0.11
−0.15	+0.075	0.14

electrons increases linearly with the atomic displacement, compared to the unperturbed initially optimized lattice positions. It is worth mentioning that, since our simulations are statically mimicking the A''_2 phononic mode, we consider relevant displacements up to 0.15 Å for Mo (0.075 Å for Te); above this threshold, we observe a sensitive stretch of the Mo–Te bond, which is a fingerprint of an incipient bond breaking (thus, far stronger than a phononic vibrational mode), which is not relevant for our analysis.

Our model is in agreement with the experimental findings and shows that a slight structural distortion can indeed cause a positive binding energy shift of the Te 4d level for tens of meVs; a linear fit of the data reported in Table 1 gives that a ∼0.01 Å shift for Mo atoms is required to reproduce the ∼10 meV shift observed in Fig. 4. In particular, this can be due to a combination of the initial state (density of states) and final state (core–hole screening) contributions, but a more thorough analysis is required to quantify the weight of both effects on the total shift observed. Interestingly, the direction of the transient core level shift reported above is in the opposite direction with respect to the position of the Te 4d line in 1T′-$MoTe_2$, as the core levels in the latter phase are found at a ∼0.6 eV lower binding energy with respect to the 2H phase.[7,42] Recent calculations by Peng *et al.*[13] demonstrate that the excited carrier density threshold for the photo-induced phase transition to occur in $MoTe_2$ is in the order of 10^{14} cm^{-2}, which is more than two orders of magnitude higher than the excitation density in our experiment; moreover, the authors show that, since the 2H-to-1T′ transition is a result of phonon softening, the transition should occur within the timescales of the lattice vibration periods (<1 ps), which is too fast to be probed with our current setup. We therefore suggest that the transient modification of the photoelectron spectra reported in this paper is rather due to a lattice distortion with a ∼600 ps time constant, supporting the theoretical hypothesis of the existence of intermediate phases along the 2H–1T′ transition.[4,43]

Conclusions

We have investigated the photo-induced dynamics of a 2H-$MoTe_2$ crystal by means of time-resolved X-ray photoemission spectroscopy. We have shown that the optical excitation generates a surface photovoltage shift of the photoemission spectra to lower binding energies, which persists for microseconds. When observing the sub-nanosecond dynamics of the system, we observed a transient shift of the Te 4d core level to higher binding energies instead, which we assigned to structural deformations in the out-of-plane direction; our DFT calculations show that an atomic displacement in the order of 0.01 Å is enough to cause a positive binding energy shift of tens of meVs, in agreement with the experiment. These results show that high-resolution time-resolved photoemission, combined with theoretical simulations, can provide valuable information not only on electronic and chemical modifications of photoexcited systems, but also on lattice distortions and phase transitions.

Author contributions

Conceptualization: MD; data curation: RC and MD; formal analysis: GG and MP; investigation: RC and MD; resources: FC and FS; visualization: RC; writing –

original draft: RC and MD; writing – review & editing: RC, FC, AM, GG, MP and MD.

Conflicts of interest

There are no conflicts to declare.

Acknowledgements

MD and RC acknowledge support from the SIR grant SUNDYN [Nr RBSI14G7TL, CUP B82I15000910001] of the Italian Ministry of Education University and Research MIUR. The work has been supported by EUROFEL MIUR Progetti Internazionali and PRIN 2017-FERMAT (Nr 2010KFY7XF). MP and GG acknowledge the availability of high-performance computing resources at Cineca under Iscra-B and Iscra-C initiatives. GG thanks the Dipartimento di Ingegneria Civile e Ambientale of the University of Perugia for allocated computing time within the project "Dipartimenti di Eccellenza 2018–2022". MP acknowledges support from the Physics Department Research Project TESLA 2021.

Notes and references

1 Q. H. Wang, K. Kalantar-Zadeh, A. Kis, J. N. Coleman and M. S. Strano, *Nat. Nanotechnol.*, 2012, **7**, 699–712.
2 W. Zheng, M. Bonn and H. I. Wang, *Nano Lett.*, 2020, **20**, 5807–5813.
3 A. Krishnamoorthy, L. Bassman, R. K. Kalia, A. Nakano, F. Shimojo and P. Vashishta, *Nanoscale*, 2018, **10**, 2742–2747.
4 A. V. Kolobov, P. Fons and J. Tominaga, *Phys. Rev. B*, 2016, **94**, 094114.
5 K.-A. N. Duerloo, Y. Li and E. J. Reed, *Nat. Commun.*, 2014, **5**, 4214.
6 D. Voiry, A. Mohite and M. Chhowalla, *Chem. Soc. Rev.*, 2015, **44**, 2702–2712.
7 S. Cho, S. Kim, J. H. Kim, J. Zhao, J. Seok, D. H. Keum, J. Baik, D. Choe, K. J. Chang, K. Suenaga, S. W. Kim, Y. H. Lee and H. Yang, *Science*, 2015, **349**, 625–628.
8 A. Britz, A. R. Attar, X. Zhang, H.-T. Chang, C. Nyby, A. Krishnamoorthy, S. H. Park, S. Kwon, M. Kim, D. Nordlund, S. Sainio, T. F. Heinz, S. R. Leone, A. M. Lindenberg, A. Nakano, P. Ajayan, P. Vashishta, D. Fritz, M.-F. Lin and U. Bergmann, *Struct. Dyn.*, 2021, **8**, 014501.
9 A. R. Attar, H. T. Chang, A. Britz, X. Zhang, M. F. Lin, A. Krishnamoorthy, T. Linker, D. Fritz, D. M. Neumark, R. K. Kalia, A. Nakano, P. Ajayan, P. Vashishta, U. Bergmann and S. R. Leone, *ACS Nano*, 2020, **14**, 15829–15840.
10 Z. Chi, H. Chen, Q. Zhao and Y.-X. Weng, *J. Chem. Phys.*, 2019, **151**, 114704.
11 Z. Wang, X. Li, G. Zhang, Y. Luo and J. Jiang, *ACS Appl. Mater. Interfaces*, 2017, **9**, 23309–23313.
12 A. Krishnamoorthy, M. F. Lin, X. Zhang, C. Weninger, R. Ma, A. Britz, C. S. Tiwary, V. Kochat, A. Apte, J. Yang, S. Park, R. Li, X. Shen, X. Wang, R. Kalia, A. Nakano, F. Shimojo, D. Fritz, U. Bergmann, P. Ajayan and P. Vashishta, *Nano Lett.*, 2019, **19**, 4981–4989.
13 B. Peng, H. Zhang, W. Chen, B. Hou, Z.-J. Qiu, H. Shao, H. Zhu, B. Monserrat, D. Fu, H. Weng and C. M. Soukoulis, *npj 2D Mater. Appl.*, 2020, **4**, 14.

14 R. Costantini, M. Stredansky, D. Cvetko, G. Kladnik, A. Verdini, P. Sigalotti, F. Cilento, F. Salvador, A. De Luisa, D. Benedetti, L. Floreano, A. Morgante, A. Cossaro and M. DellAngela, *J. Electron Spectrosc. Relat. Phenom.*, 2018, **229**, 7–12.
15 R. Costantini, R. Faber, A. Cossaro, L. Floreano, A. Verdini, C. Hättig, A. Morgante, S. Coriani and M. DellAngela, *Commun. Phys.*, 2019, **2**, 56.
16 G. Kresse and J. Hafner, *Phys. Rev. B: Condens. Matter Mater. Phys.*, 1993, **48**, 13115–13118.
17 G. Kresse and J. Furthmüller, *Phys. Rev. B: Condens. Matter Mater. Phys.*, 1996, **54**, 11169–11186.
18 G. Kresse and J. Hafner, *Phys. Rev. B: Condens. Matter Mater. Phys.*, 1994, **49**, 14251–14269.
19 G. Kresse and J. Furthmüller, *Comput. Mater. Sci.*, 1996, **6**, 15–50.
20 J. P. Perdew, K. Burke and M. Ernzerhof, *Phys. Rev. Lett.*, 1996, 77, 3865–3868.
21 P. E. Blöchl, *Phys. Rev. B: Condens. Matter Mater. Phys.*, 1994, **50**, 17953–17979.
22 S. Grimme, J. Antony, S. Ehrlich and H. Krieg, *J. Chem. Phys.*, 2010, **132**, 154104.
23 L. Köhler and G. Kresse, *Phys. Rev. B: Condens. Matter Mater. Phys.*, 2004, **70**, 165405.
24 Y. Tan, F. Luo, M. Zhu, X. Xu, Y. Ye, B. Li, G. Wang, W. Luo, X. Zheng, N. Wu, Y. Yu, S. Qin and X.-A. Zhang, *Nanoscale*, 2018, **10**, 19964–19971.
25 C. Si, D. Choe, W. Xie, H. Wang, Z. Sun, J. Bang and S. Zhang, *Nano Lett.*, 2019, **19**, 3612–3617.
26 J. Liu, Y. Wang, X. Xiao, K. Zhang, N. Guo, Y. Jia, S. Zhou, Y. Wu, Q. Li and L. Xiao, *Nanoscale Res. Lett.*, 2018, **13**, 291.
27 S. Tanaka, S. D. More, J. Murakami, M. Itoh, Y. Fujii and M. Kamada, *Phys. Rev. B: Condens. Matter Mater. Phys.*, 2001, **64**, 155308.
28 K. Wang, Y. Feng, C. Chang, J. Zhan, C. Wang, Q. Zhao, J. N. Coleman, L. Zhang, W. J. Blau and J. Wang, *Nanoscale*, 2014, **6**, 10530–10535.
29 A. R. Beal and H. P. Hughes, *J. Phys. C: Solid State Phys.*, 1979, **12**, 881–890.
30 A. J. Grant, T. M. Griffiths, G. D. Pitt and A. D. Yoffe, *J. Phys. C: Solid State Phys.*, 1975, **8**, L17–L23.
31 J.-H. Kim, M. R. Bergren, J. C. Park, S. Adhikari, M. Lorke, T. Frauenheim, D.-H. Choe, B. Kim, H. Choi, T. Gregorkiewicz and Y. H. Lee, *Nat. Commun.*, 2019, **10**, 5488.
32 R. Costantini, A. Morgante and M. DellAngela, *J. Electron Spectrosc. Relat. Phenom.*, 2022, **254**, 147141.
33 B. Radisavljevic and A. Kis, *Nat. Mater.*, 2013, **12**, 815–820.
34 A. Chernikov, C. Ruppert, H. M. Hill, A. F. Rigosi and T. F. Heinz, *Nat. Photonics*, 2015, **9**, 466–470.
35 N. L. A. N. Sorgenfrei, E. Giangrisostomi, R. M. Jay, D. Kühn, S. Neppl, R. Ovsyannikov, H. Sezen, S. Svensson and A. Föhlisch, *Adv. Mater.*, 2021, **33**, 2006957.
36 S. Tokudomi, J. Azuma, K. Takahashi and M. Kamada, *J. Phys. Soc. Jpn.*, 2008, **77**, 014711.
37 D. Bröcker, T. Gießel and W. Widdra, *Chem. Phys.*, 2004, **299**, 247–251.
38 A. Shavorskiy, S. Neppl, D. S. Slaughter, J. P. Cryan, K. R. Siefermann, F. Weise, M.-F. Lin, C. Bacellar, M. P. Ziemkiewicz, I. Zegkinoglou, M. W. Fraund, C. Khurmi, M. P. Hertlein, T. W. Wright, N. Huse, R. W. Schoenlein,

T. Tyliszczak, G. Coslovich, J. Robinson, R. A. Kaindl, B. S. Rude, A. Ölsner, S. Mähl, H. Bluhm and O. Gessner, *Rev. Sci. Instrum.*, 2014, **85**, 093102.
39 S. Hellmann, K. Rossnagel, M. Marczynski-Bühlow and L. Kipp, *Phys. Rev. B: Condens. Matter Mater. Phys.*, 2009, **79**, 035402.
40 M. DellAngela, T. Anniyev, M. Beye, R. Coffee, A. Föhlisch, J. Gladh, S. Kaya, T. Katayama, O. Krupin, A. Nilsson, D. Nordlund, W. F. Schlotter, J. A. Sellberg, F. Sorgenfrei, J. J. Turner, H. Öström, H. Ogasawara, M. Wolf and W. Wurth, *Struct. Dyn.*, 2015, **2**, 025101.
41 D. Riffe, W. Hale, B. Kim and J. Erskine, *Phys. Rev. B: Condens. Matter Mater. Phys.*, 1996, **54**, 17118–17122.
42 J. R. Shallenberger, R. Katz and Z. Mao, *Surf. Sci. Spectra*, 2021, **28**, 024001.
43 H. H. Huang, X. Fan, D. J. Singh, H. Chen, Q. Jiang and W. T. Zheng, *Phys. Chem. Chem. Phys.*, 2016, **18**, 4086–4094.